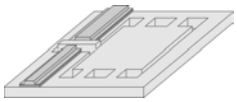

2.1 Introduction

In broadband communication systems, information is coded in the form of light pulses, as shown in fig 2.1a. These pulses are transmitted, through waveguiding structures, from the source to the receiver, where the information is decoded. As the number of pulses per unit time that can be sent and decoded increases, the system transmission capacity is greatly enhanced, being able to transmit larger quantity of information. However, there exist some limitations on the pulse frequency due to optical signal distortion as it travels along a guiding structure. The consequence of this distortion can be seen in fig 2.1b. As the distance (or propagation time) increases, the pulse progressively broadens. Thus, the resolution (defined as the difference between the maximum and the minimum intensity value) decreases, being more difficult to detect the pulses at the detector. For large broadening, it becomes nearly impossible to differentiate two consecutive pulses, as shown in fig, 2.1c.

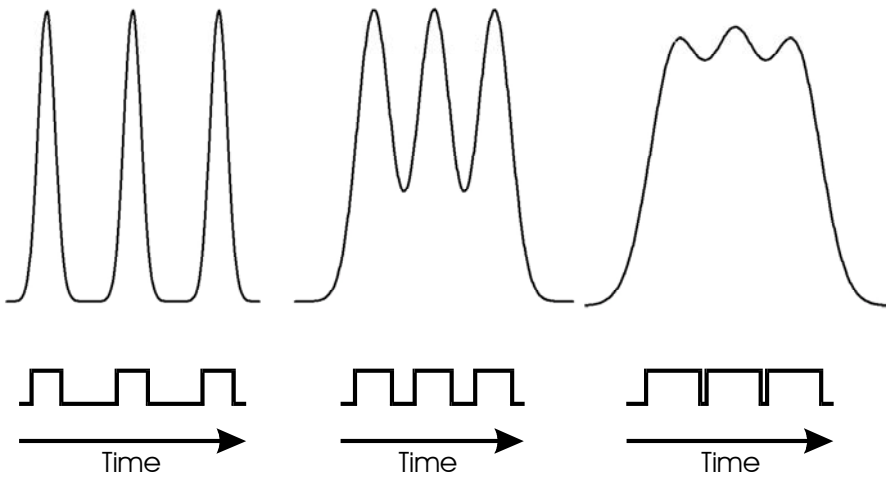

Fig 2.1.: Pulse resolution lowering due to broadening as a function of time (or distance).

As previously mentioned, when a light pulse is injected in a multimode fiber optic or a waveguide, it broadens as a function of time and propagation distance. This behavior is mainly due to the i*ntermodal dispersion* and it is a direct consequence of the fact that each mode propagates at a different speed along the guiding structure. Thus, even if two closer pulses can be well resolved at the input end, because of the

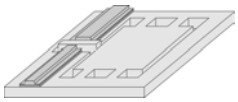

broadening, they may not be so at the receiver. In those situations where the output pulses are not resolvable, the information cannot be retrieved. This dispersion can be overcame by single-mode operation. Actually, the state-of-art in broadband telecommunications systems operating over long distances do actually use this principle of operation.

The above description does not mean that single mode waveguides do not suffer from dispersion. It has to be noted that all light sources have a central wavelength value λ_0 but also have a certain width $\Delta\lambda$. Thus, each wavelength within this width also takes a different time to arrive at the receiver, causing a pulse broadening. This broadening due to the spectral width of the light source is called *intramodal dispersion*.

There also exist some other properties that can cause pulse broadening. If the waveguide optical properties (refractive index and absorption coefficient) have a non-linear response with λ, or even if, due to difficulties on the fabrication process, those layers comprising the guiding structure are not homogeneous, linear and isotropic (*HLI materials)*, the propagation along the waveguides will depend on its behavior with λ. Thus, a broadening due to *material dispersion* can also be observed.

Finally, the goodness of any guiding structure clearly depends on its capacity of confining the light with as lower losses as possible. There exists several optical properties that allows obtaining confinement (as could be *Total Internal Reflection* or *AntiResonant Reflecting Optical Waveguides*), but in all of them, each mode reaches the boundary between the core layer and the adjacent layers with a certain angle. Even if the structure is single-mode, this angle is a function of λ for a given waveguide geometry and refractive index values. Thus, the w*aveguide dispersion* produces a λ-dependent delay along the guiding structure, which increases as $\Delta\lambda$ spans from the central value λ_0.

As can be observed in table 2.1, in multimode guiding structures, the intermodal dispersion prevails and other dispersion effects can be neglected. This fact is the former drawback that prevents the application of this kind of structures in telecommunications. There are, however, some other application fields where these guiding structures can be used, as it will be explained later on. For single moded waveguides fabricated with LHI materials and with a coherent light source, there only exists intramodal dispersion, which is much lower and the light pulses can be closely

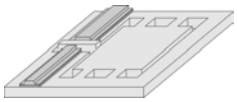

transmitted, increasing the overall information transmission speed. If incoherent light sources are used, the dispersion on the waveguide and on the material should also be studied.

	Single-mode	**Multimode**
I*ntermodal dispersion*	Does not exist	Important
Intramodal dispersion	Important	Neglectable
Material dispersion	Variable	Neglectable*
W*aveguide dispersion*	Variable	Neglectable

* Except for highly non-linear media

Table 2.1: Different dispersion effects that cause pulse broadening on light guiding structures.

At this point, it will be useful knowing which waveguide configurations are the most appropriate for single-mode behavior. There exist several optical principles in which guiding structures could be based on. Between them, Total Internal Reflection (TIR) and AntiResonant Reflecting Optical Waveguides (ARROW) configurations could be highlighted, since they are the most versatile, simple and robust.

The simplest Total Internal Reflection waveguides consist on two layers with different refractive index. Single-mode behavior can be obtained either with a small refractive index difference between the core and the buffer layer (fig. 2.2a) or with a thin core (fig. 2.2b). Comparison between TIR waveguides can be done by defining the external asymmetry parameter as $\Delta n_{ce}= n_c - n_{ext}$, where n_c is the refractive index of the core and n_{ext} is that of the external media. Hence, for thick waveguides, Δn_{ce} has to be small for single mode waveguides. On the contrary, if the core is thin, high Δn_{ce} values can be used while keeping the expecting modal properties. How these values are correlated has previously been studied in **[1]**. Problems with this configuration arise during the fabrication and the characterization. Firstly, for waveguides with small Δn_{ce} require thick layers, which frequently crack if the deposition (or growth) conditions are not optimized. Furthermore, they require a small difference between the refractive indexes, that is, the necessary equipment must give a thick layer while keeping constant its composition. These strong requirements need extremely complex systems that reduce the possibility of mass-production.

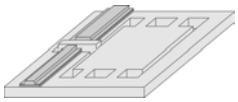

Although it is much easier to fabricate a TIR waveguide with a high Δn_{ce}, problems arise during the characterization. Light is commonly injected by end-fire coupling from a single-mode optical fiber with a diameter of 4 μm. As an example, the core of a waveguide with Δn_{ce}=2.00 (as could be a Si_3N_4 waveguide), must not exceed 0.1μm for having single-mode operation. This strong difference between the areas of the guiding structures causes high losses during injection if end-fire coupling is used. Furthermore, core waveguides are commonly etched so as to have cross-section confinement, as it will be discussed later. For keeping single-mode operation, this etch must not exceed 5nm. Although it can be done with standard lithography and etching processes, waveguides cannot be seen at naked eye and it obviously is a major drawback for alignment of integrated optical devices, light sources and photodetectors.

The major advantage of ARROW structures (fig. 2.2c and d) is that, due to its principle of operation, their modal properties does not depend on the core thickness, but on the antireflective pair located just beneath the core. Hence, it is possible to obtain waveguides with a core thicknesses of the same magnitude as compared to the input fiber optics while keeping its single-mode properties unchanged. This behavior is observed in fig 2.2c and d, where the first mode in both structures has a deep penetration into the substrate, as compared to the fundamental mode, which has not. They also have several additional properties that will be discussed in the next section.

2.2 ARROW Waveguides

During the last fifty years, research on microelectronics has overcome the most optimistic expectations, both in achievements and in new equipment. Integrated optics is still far from microelectronics, but it is expected to progress much faster since, instead of developing new equipment, the previously developed systems can be adapted so as to provide good results in integrated optics. It has to be taken into account, however, that the main material used in microelectronics is silicon, which is absorbent for wavelengths below 1.12μm. Then, the first was the design of a new waveguide that could operate in the visible region with acceptable absorption losses while keeping its single-mode behavior.

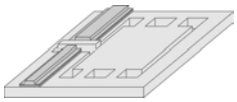

The response of such strong requirements was the development of ARROW-A **[2]** and ARROW-B **[3]** waveguides in 1986 and 1989, respectively. Their basic configuration has previously been presented in fig 2.2. They consist on two different layers placed just below the core. Its refractive index and thickness has to be chosen, for a given working wavelength, so as provide very high reflection at the core-1st cladding (d_1) interface. At the upper air-core interface still undergoes total internal reflection.

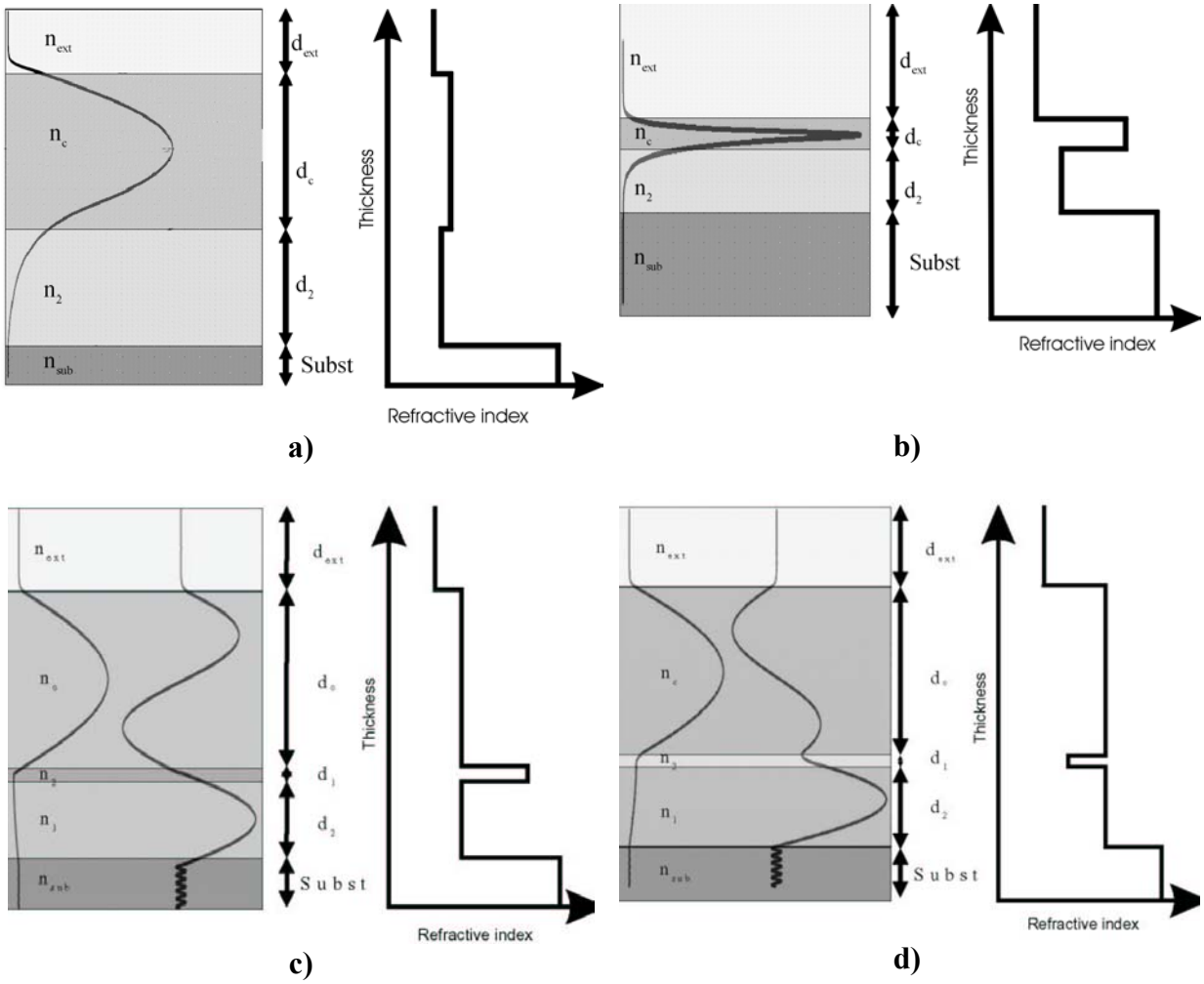

Fig 2.2.: Different waveguide single-mode configurations a) TIR waveguide with small refractive index difference between the core and the underlayer. b) TIR waveguide with high refractive index difference. c) fundamental and first mode of an ARROW-A waveguide. c) fundamental and first mode of an ARROW-B waveguide.

The antiresonant pair (d_1 and d_2) has the transmission properties of two Fabry-Perot resonators. Hence, high reflection happens at its antiresonant wavelengths. If each layer is sintonized so as to have the same transmission properties, a very high reflection (>99.96%) will be achieved. Due to the fact that the principle of operation relies on the properly phased reflections at each boundary, it could be thought that the fabrication conditions of these structures are extremely strict and that they only work over a very narrow band of wavelengths. In order to confirm or deny this point, theoretical expressions of the sintonized layer thicknesses as a function of the working parameters should be derived.

2.2.1 Theoretical Expressions

As presented in fig. 2.3, and using ray-tracing optics, the phase difference between the ray reflected at the core-1st cladding interface (A) and the ray reflected at the 1st cladding-2nd cladding interface (B) is given by:

$$\delta_1 = kn_1 d_1 \cos(\theta_1) \tag{2.1}$$

where n_1 and d_1 are the refractive index and thickness of the 1st cladding layer, θ_1 is the angle at which light propagation through the core is refracted in the 1st cladding layer in reference to the normal and k is the wavenumber.

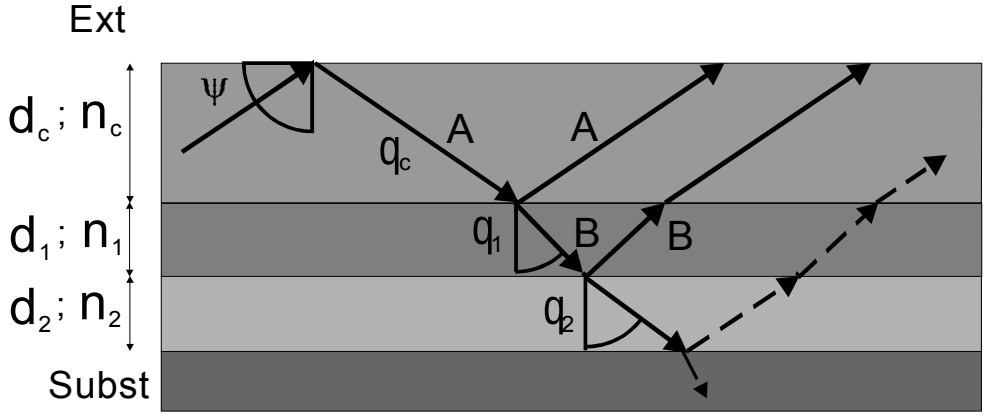

Fig 2.3.: Ray-tracing scheme in an ARROW-A waveguide, where the different rays that provide antiresonance-based confinement are plotted (A & B).

On the basis of the same deductions, inside the core the phase difference is:

$$\delta_c = kn_c d_c \cos(\theta_{c,m}) \tag{2.2}$$

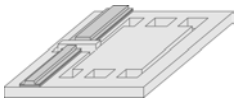

where n_c and d_c are the refractive index of the core and $\theta_{c,m}$ is the angle at which each mode m is reflected at the core boundaries.

As can be seen from the previous expression, δ_c depends on the light propagating angle, which is different for every mode. The propagation constant of the m^{th} mode (β_m) can also be given as a function of $\theta_{c,m}$, and has the expression.

$$\beta_m = kn_c \cos\psi_m = kn_c \operatorname{sen}\theta_{c,m} \tag{2.3}$$

if antiresonance is imposed, then ($\delta_c = (2g+1)\pi/2$, g=0, 1, 2,...). Applying this condition to ec. (2.2) one obtains the incidence angle for each layer

$$\begin{aligned} \cos\theta_c &= \frac{(g+1)\lambda}{2d_c n_c} \\ \cos\theta_1 &= \sqrt{1-\left(\frac{n_c}{n_1}\right)^2+\left(\frac{(g+1)\lambda}{2d_c n_1}\right)^2} \\ \cos\theta_2 &= \sqrt{1-\left(\frac{n_c}{n_2}\right)^2+\left(\frac{(g+1)\lambda}{2d_c n_2}\right)^2} \end{aligned} \tag{2.4}$$

These expressions can be introduced to the well-known reflection coefficients **[4]** so as to obtain the reflectivity (R) expression for any polarization:

$$R = \frac{r_{1\to2}^2 + r_{2\to3}^2 + 2r_{1\to2}r_{2\to3}\cos(2\delta_c)}{1 + r_{1\to2}^2 r_{2\to3}^2 + 2r_{1\to2}r_{2\to3}\cos(2\delta_c)} \tag{2.5}$$

where $r_{i\to j}$ stands for the reflection coefficient at the boundary between the layers *i* and *j* (i=1,2; j=2,3).

In fig 2.4 the ec. (2.5) as a function of d_1 has been plotted for several core thicknesses. As can be observed, there exist some periodic narrow values of d_1 where a minimum of reflectivity is obtained. These values correspond to the Fabry-Perot resonance values. On the contrary, the regions where reflectivity is close to unity are broad, corresponding to antiresonance values. Hence, and as far as fabrication is concerned, layer thicknesses have a high degree of tolerance. It also can be observed how reflectivity decreases when the core size is reduced. This fact is comparable to the finesse decrease in a Fabry-Perot **[5]**. Core properties (d_c and n_c) are, for a given wavelength, the responsible of the light confinement inside the guiding structure. If, keeping constant the refractive index, the core thickness is progressively reduced, the

confinement is also reduced and the modes propagating through the waveguide partially travels outside the structure. This portion of electromagnetic field propagating beyond the core boundary layers is commonly known as the evanescent field and its magnitude increases as the core thickness decreases. It can be understood as a decrease of the reflectivity mirror properties. Hence, one realizes that the decrease in the core thicknesses causes the same effect than the finesse decrease in a Fabry-Perot Interferometer.

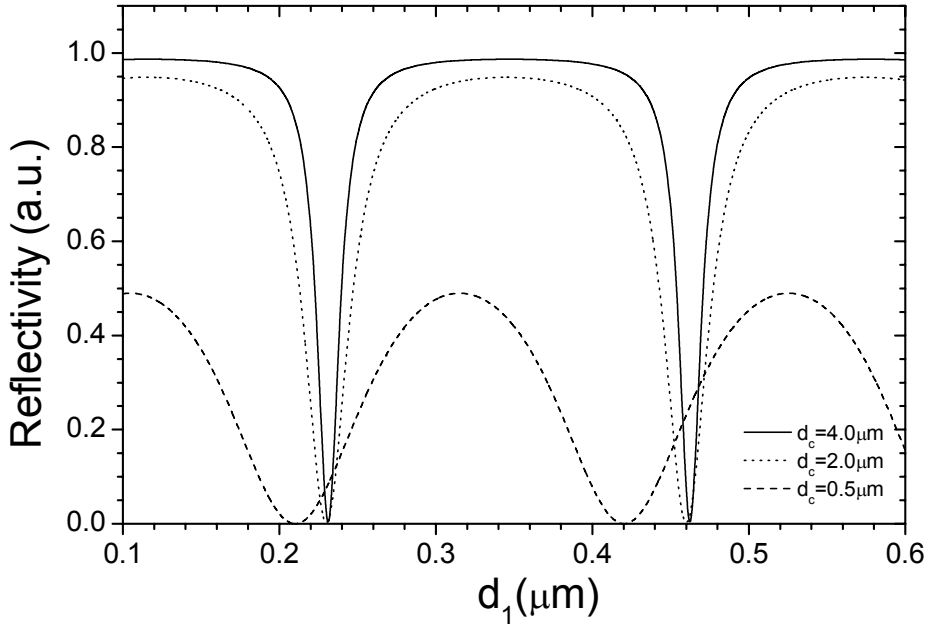

Fig 2.4.: Reflectivity vs. d_1 for three different core thickness d_c in an ARROW-A structure, with refractive index values $n_c=n_2=1.46$, $n_1=2.00$ and working wavelength $\lambda=633$nm.

Minimizing ec. (2.5), it is possible to express the values where d_1 has a maximum of reflectivity as a function of the rest of the parameters involved. It can be written in the form:

$$d_1 = \frac{(2g+1)\lambda}{4n_1}\left[1-\left(\frac{n_c}{n_1}\right)^2+\left(\frac{(m+1)\lambda}{2n_1 d_c}\right)^2\right]^{-1/2} \qquad (2.6)$$

In all previous calculations, it has been supposed for simplification that reflections were produced at the boundaries, that is, the effect of the evanescent field penetration on the surrounding media was neglected. However, this approximation

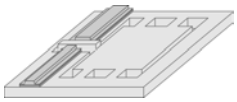

could be too strong in poorly confining waveguides (for example, with a thin core). This effect can be considered with the introduction of the so-called Goos-Hänchen shift **[6]**. This effect causes the replacement of d_c in all previous equations by an effective core thickness d_{ce}, given by

$$d_{ce} \approx d_c + \varepsilon_0 \frac{\lambda}{2\pi\sqrt{n_c^2 - n_{ext}^2}}$$
$$\varepsilon_0 = \begin{cases} 1 & \text{modes } TE \\ \left(\frac{n_{ext}}{n_c}\right)^2 & \text{modes } TM \end{cases} \tag{2.7}$$

Generalizing the previous results, it could be affirmed that, for a given layer *i* with refractive index n_i, its antiresonant thickness will be

$$\mathrm{d_i} = \frac{(2g+1)\lambda}{4n_i}\left[1 - \left(\frac{n_c}{n_i}\right)^2 + \left(\frac{(m+1)\lambda}{2n_1 d_{ce}}\right)^2\right]^{-1/2} \tag{2.8}$$

If the 2nd cladding refractive index is equal to the core refractive index ($n_2=n_c$), at the 1st antiresonant condition (g=0) and for the fundamental mode (m=0) equation 2.8 is greatly simplified

$$\mathrm{d}_2^{n_2=n_c} = \frac{(2g+1)d_{ce}}{2} \tag{2.9}$$

Attenuation of the several modes, defined as the power loss per unit propagation length can be related to the reflectivity **[7]** as

$$\alpha_m\left(\frac{dB}{cm}\right) = 2.17(1-R)\frac{1}{d_{ce}}\sqrt{\left(\frac{2n_c d_{ce}}{(m+1)\lambda}\right)^2 - 1} \tag{2.10}$$

Evaluating this expression as a function of d_1, as shown in fig 2.5, allows confirming that it is technologically simple to achieve the necessary thicknesses so as to provide the optimum antiresonant layers.

Summing up, it has been observed how in ARROW-A structures light propagates through the core by repeating TIR at the upper air-core boundary and ultrahigh reflection (>99.96%) for the TE_0 due to the antiresonant interference claddings. The amount of power that is not reflected corresponds to radiation loss. Hence, any ARROW mode has a certain degree of losses. Properly speaking, instead of

ARROW modes, it should be written quasi-guided or leaky modes. However, for simplification on labeling and since their behavior actually is identical to a standard mode, we always describe them as ARROW modes.

It can be observed that the theoretical study done basically corresponds to a multiple Fresnel reflection. Thus, on the basis of Fresnel coefficients, attenuation should strongly depend on light polarization. Instead of repeating the same analytical calculations for the TM modes, it will be easier to contrast this fact during the numerical simulations.

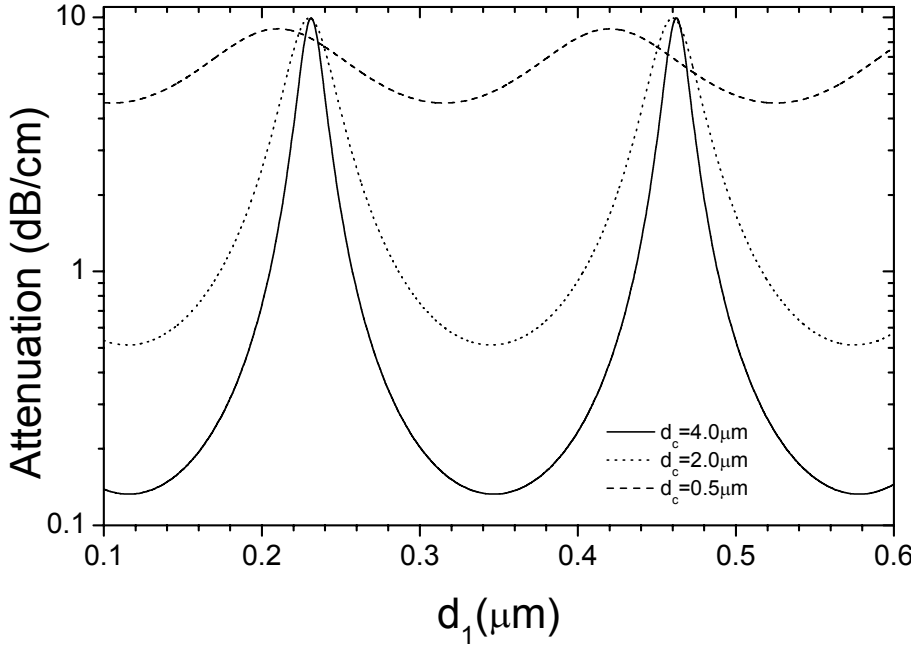

Fig 2.5.: Attenuation vs. d_1 for three different core thickness d_c in an ARROW-A structure, with the same refractive index values as the previous figure and working wavelength. Maximum attenuation can be observed at the reflectivity minimums.

On the other hand, in ARROW-B waveguides, schematically presented in fig. 2.2d, the refractive index of the first cladding is the smallest on the structure (except air). Then, if this layer is thick enough, this waveguide will behave as a TIR waveguide and its modal properties will depend on the core thickness and the refractive indexes of the layers, as it happens with all TIR waveguides. However, if d_1 were made thin enough so as to permit that the evanescent tail reaches the second cladding, it would interfere in this layer. Moreover, if it is taken into account that the first reflection at the

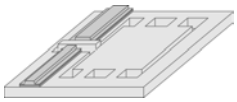

core-1st cladding is the most important on light confinement and interference does not have a strong dependence with polarization, attenuation in ARROW-B should be less dependent on polarization as compared to ARROW-A. Both ARROW waveguides considered, however, should have the same modal properties: higher order modes should be filtered out since the antiresonant pair would only have high reflectivity for the TE_0 mode.

In order to confirm the above-predicted behavior, it could be extremely useful to use a numerical analysis. Although it could also be possible to do it analytically, the optimization of ARROW structures will be clearer and less tedious with a numerical approach. Furthermore, as it will be studied in the next section, there exist several geometries where analytical calculus have a high degree of complexity or simply does not have an analytical solution.

2.2.2 Numerical Simulations

Up to this point, only a brief approach to some of the optical properties of slab ARROW-A structures has been done. Furthermore, as previously mentioned, slab structures are generally not used in integrated optics, since it does not allow a dense integration of optical devices on the same chip. Hence, ARROW core is partially etched so as to provide cross-section confinement. Obtaining the appropriate boundary conditions for this geometry is extremely difficult, although it has been solved for some particular cases **[8]**. Thus, if an optimization of these waveguides wants to be done, it is more useful to use a numerical simulation program instead of analytical deduction.

There exist several numerical simulation methods that provide, with a different degree of accuracy, the optical constants and the propagation property of any integrated optical device. The first one was developed for squared cross-section waveguides **[8]**, lately modified and renamed as *Effective Index Method (EIM)* **[9]**. Although both methods are simple and fast, the propagation constant values that these methods provide do not match with the experimental results as the modes are less confined, that is, as they approaches the *cutoff condition* **[10]**.

If inhomogeneous and anisotropic guiding structures with arbitrary cross section want to be studied, it becomes necessary to use more complex simulation methods, as could be the *Finite Elements Method (FEM)* **[11]** or the *Finite Difference*

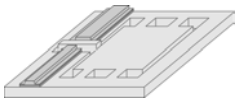

Method (FDM) **[12]**. Both are based on the waveguide cross-section division in a certain number of regions, where, under the application of the appropriate boundary conditions, *the wave equation* can be numerically solved inside every region (FEM) or at every point (FDM). Both methods are able to provide the propagation constant, the attenuation and radiation losses, the evanescent field and their modal properties. Although some FEM methods are also able to provide the field amplitude evolution along the propagation direction, generally it has to be implemented separately. The most common method for analyzing the field evolution along the propagating direction is the *Beam Propagation Method (BPM)* **[13]**, which, for a given amplitude profile at z=0, is able to determine its shape at a certain distance z_f provided by the user. There exist several variations of BPM, in order to include 2D confinement, backscattering, wide angle propagation or even bent waveguides. Depending on the parameters under study, it would be necessary to choose the most appropriate BPM algorithms. Normally, it would be extremely useful to have information concerning the evolution of a 2D profile along the propagation axis. Unfortunately, a 2D-BPM requires an excessively long computing time. What is normally done, working far from cutoff condition, is reducing one dimension of the device, through effective index method, and then use the standard BPM algorithms. This method is generally called FDM-(EIM)BPM or FEM-(EIM)BPM.

Particularly, in our case, it has been developed a FDM method with a Non-Uniform Mesh (NU-FDM) **[12]**. The non-uniformity of the mesh allows obtaining the same results as the uniform mesh, but with much lesser computational time. The density of analysis points is higher near boundary regions or where it is needed. On the contrary, it is sparse where the layers are locally homogeneous. The non-uniformity of the mesh is particularly important in those structures with high difference between the layer thicknesses, as could be ARROW waveguides.

Before starting analyzing the properties of Rib-ARROW waveguides, it will be of worth confirming the expected behavior of slab structures. Moreover, its operation principle does not depend on the rib as far as layer thicknesses or refractive index differences are concerned. Firstly, the thickness of the different layers will be optimized in order to minimize the attenuation losses for the TE_0 mode. Once determined the layer

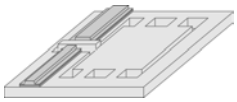

dimensions, its stability, as a function of refractive index variations will also be studied. Finally, rib will be introduced so as to analyze the change on the modal properties as the etching is increased. During all the following simulations the working wavelength will be fixed at 633nm.

For this analysis, it becomes useful to define the external and internal asymmetry coefficients, being respectively $\Delta n_{ce}= n_c-n_{ext}$ and $\Delta n_{c2}=n_c-n_2$. While the former parameter will provide information concerning the confinement degree of the modes on the structure, the latter will be responsible of the number of guided modes. The letter between brackets after Δn_{ci} will be (A) for an ARROW-A or (B) for an ARROW-B.

In the previous analytical calculations, it was possible to obtain a certain value for the first cladding thickness that assured antiresonance. It could be a good starting point when optimizing the second cladding to consider the obtained d_1 value as correct. Lately, a comparison between the analytical and the numerical results will be done so as to confirm the simulation method. From the analytical results obtained in fig. 2.4 and 2.5, it will become logical to consider core thicknesses above 3µm. Reduction of the core dimensions will also be studied afterwards. At this point, we will consider d_c=4µm, Δn_{c2}=0 for both structures, while d_1=0.12µm, Δn_{ce}= 0.46 will be chosen for ARROW-A; d_1=0.5µm, Δn_{ce}= 0.56 will be the parameters for ARROW-B. Reasons why choosing the core thickness and the 1st cladding for ARROW-A are clear from the previous analysis, as they also are, in according to equation 2.9, the election of Δn_{c2}=0. Δn_{ce} values are not extremely important at this point, since the effects on its variation are not under study yet. However, their values have been chosen following two main criteria: 1. Ability to obtain materials with the expected internal and external asymmetry coefficients with the available technology. 2. Capability to compare the results obtained with the literature. Finally, d_1 value for ARROW-B structure has been chosen considering the property that it should have, as it was described at the end of the previous section: thin enough so as to permit the evanescent tail to reach the second cladding.

Generally, we will focus our study in two main properties of the guiding structures: attenuation (also called radiation loss) and dispersion (effective refractive index variation). While the former will provide essential information concerning the

amount of power that will be obtained at the output of the device, the latter allows determining the optical properties of each mode. If necessary, a third property, the evanescent field, will be included as a complement of the previous. It will be particularly useful when the confinement or the coupling between waveguides were to be studied.

Attenuation and dispersion as a function of d_2 for TE and TM polarization can be seen in fig. 2.6. As expected, minimum radiation losses, with $\Delta n_{c2}=0$, are obtained when $d_2=d_c/2$, as predicted in eq. (2.9). As a rule, when d_2 is an odd multiple of $d_c/2$, minimum attenuation for even order modes and maximum attenuation for odd modes is obtained. On the contrary, when d_2 is a multiple of d_c, the radiation losses of even order modes reaches its maximum, since it behaves as a vertical directional coupler **[14]**. It can be observed how the most significant difference between both structures is its polarization dependence: the attenuation of TM_0 in ARROW-A is at least two orders of magnitude higher as compared to TE_0, confirming the previously described multiple Fresnel reflection principle. On the contrary, in ARROW-B configuration, a lower dependence on polarization is observed. Although this behavior could be considered as a limitation for some applications, there are others where the non-polarization dependence structures greatly simplifies the device configuration. For example it allows working with incoherent light sources or, at least, not to worry about the light polarization that is injected at the device input.

Finally, it can be observed how the dispersion behavior is identical for both structures and for both polarizations: there is no modal transition for the lowest order mode when d_2 is varied between 0 and 3µm. However, higher order modes present modal transition at d_2 thicknesses where resonant condition is obtained.

Further simulations will always consider the results obtained in the figure 2.6. That is, the second cladding thickness will be sintonized at $d_c/2$ in order to assure minimum attenuation from the second cladding layer.

In the previous section, we have found the analytical expression for the minimum radiation losses for ARROW-A waveguides and we have also seen that the region were this condition is achieved is significantly broad. For ARROW-B, however, only a qualitatively analysis has been done according to its internal and external

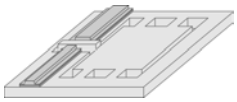

asymmetry parameters. Following the same optimization steps of the second cladding layer, the behavior of the attenuation and the dispersion for both ARROW structures and polarization as a function of the first cladding thickness is presented in fig 2.7 and 2.8. The same asymmetry parameters as the previous figure have been chosen at the same wavelength and with $d_2=d_c/2$. So far, the single difference between ARROW-A and ARROW-B structures were the non-polarization selectivity of the latter, since the attenuation and dispersion had the same overall properties. It can be observed in figs 2.7 and 2.8 how major differences between them arise due to the different asymmetry values of each structure.

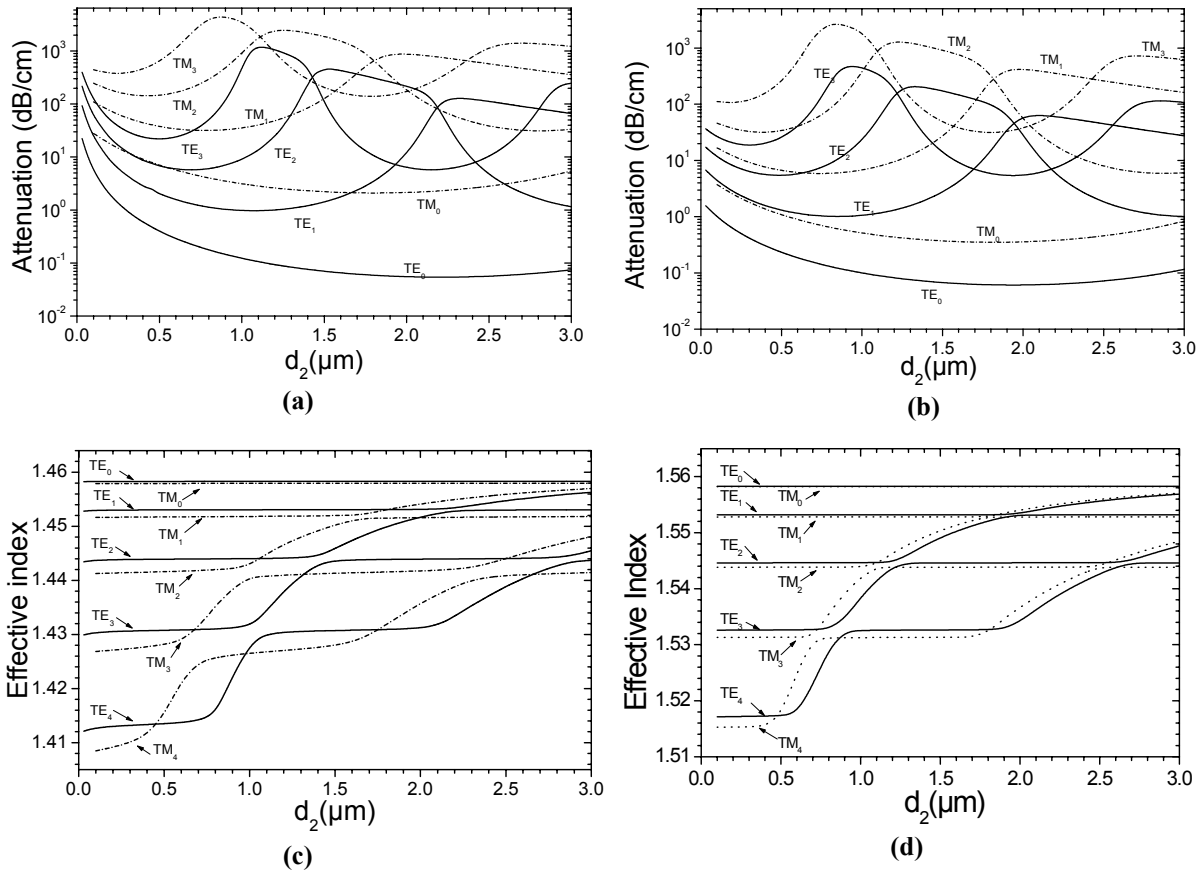

Fig 2.6.: Attenuation and dispersion for the lower TE and TM modes vs. d_2 for ARROW-A (a & c) and ARROW-B (b &d) structures. In both d_c=4μm; λ=633nm; Δn_{c2}=0. For ARROW-A Δn_{ce}=0.46(A) and d_1=0.12μm, while Δn_{ce}=0.56(B) and d_1=0.5μm were for ARROW-B

Confirming the analytical results obtained in the previous section, radiation losses in ARROW-A exhibit periodicity as a function of d_1, as shown in fig 2.7a. The

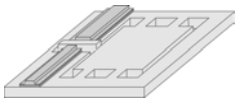

loss of even order modes has its minimum value at the antiresonant conditions (eq. 2.6). Before analyzing the effective refractive index properties, it has to be noted that this structure is able to support two types of guided modes. If $n_c<n_{eff}<n_1$, modes correspond to first cladding layer, which are TIR modes due to the higher refractive index value of this layer. When $n_{ext}<n_{eff}<n_c$ the ARROW modes are obtained. As observed in fig 2.7b, these modes are leaky modes into which TIR 1st cladding modes are transformed when they reach their cutoffs. The resonant values of d_1, where maximums in attenuation are achieved, correspond to this cutoff condition. This supposition is confirmed by the evanescent field magnitude, shown in fig. 2.7c. It is observed how a sharp variation of the evanescent field is produced at the antiresonance values. Since there has been no variation on the upper boundary layer, there is no reason why supposing that the variation observed in fig 2.7c is due to modifications of the upper interface. On the contrary, as d_1 deviates from antiresonance, the TE_0 mode is less confined and the effective refractive index tends to its cutoff condition. Finally, when this situation is achieved, an overall modal transition is produced, changing TE_i by TE_{i-1} (i=1,..N). If it is considered that higher modes have lower confinement factor in both layers, it becomes logical that at near values above the cutoff condition, the evanescent field to be maximum, since a modal transition has just produced.

Finally, as it is seen in fig. 2.7, TM modes also have at least two orders of magnitude higher attenuation as compared to TE, but their overall behavior is exactly the same: periodicity and sharp attenuation maximums as a function of d_1.

Fig. 2.8 shows the attenuation (a), the dispersion (b) and the evanescent field (c) characteristics of ARROW-B as a function of d_1 for both polarisations. It can be observed how all their optical properties are completely different from the previously studied in ARROW-A structures, being of special significance the lack of periodicity of the parameters under study: attenuation monotonically decreases when d_1 increases for all modes and for both polarisations. Dispersion values converge asymptotically to constant values as d_1 increases. Finally, in fig. 2.8c it can be observed how after a fast increase, the evanescent field reaches a nearly constant value as a function of d_1. This behavior can be clearly understood if it is taken into account that ARROW-B modes are obtained when $n_1<n_{eff}<n_c$.